

Nonlinear spectroscopy of three-photon excitation of cesium Rydberg atoms in vapor cell

Jiabei Fan(樊佳蓓), Yunhui He(何云辉), Yuechun Jiao(焦月春), Liping Hao(郝丽萍), Jianming Zhao(赵建明), and Suotang Jia(贾锁堂)

Citation: Chin. Phys. B, 2021, 30 (**3**): 034207. DOI: 10.1088/1674-1056/abca25
Journal homepage: http://cpb.iphy.ac.cn; http://iopscience.iop.org/cpb

What follows is a list of articles you may be interested in

Research progress of third-order optical nonlinearity of chalcogenide glasses

Xiao-Yu Zhang(张潇予), Fei-Fei Chen(陈飞飞), Xiang-Hua Zhang(章向华), Wei Ji(季伟)
Chin. Phys. B, 2018, 27 (**8**): 084208. DOI: 10.1088/1674-1056/27/8/084208

Coherently induced grating in refractive index enhanced medium

Zhuan-Zhuan Liu(刘撰撰), Yu-Yuan Chen(陈煜远), Jia-Yu Yuan(原佳宇), Ren-Gang Wan(万仁刚)
Chin. Phys. B, 2017, 26 (**12**): 124209. DOI: 10.1088/1674-1056/26/12/124209

Retrieval of high-order susceptibilities of nonlinear metamaterials

Zhi-Yu Wang(王志宇), Jin-Peng Qiu(邱仅朋), Hua Chen(陈华), Jiong-Jiong Mo(莫炯炯), Fa-Xin Yu(郁发新)
Chin. Phys. B, 2017, 26 (**9**): 094207. DOI: 10.1088/1674-1056/26/9/094207

Electromagnetically induced grating in a thermal N-type four-level atomic system

Ya-Bin Dong(董雅宾), Jun-Yan Li(李俊燕), Zhi-Ying Zhou(周志英)
Chin. Phys. B, 2017, 26 (**1**): 014202. DOI: 10.1088/1674-1056/26/1/014202

Measurement of the argon-gas-induced broadening and line shifting of the barium Rydberg level 6s24d $^1D_2$ by two-photon resonant nondegenerate four-wave mixing

Sun Jiang, Xiong Zhi-Qiang, Sun Juan, Wang Ying, Su Hong-Xin
Chin. Phys. B, 2012, 21 (**6**): 064215. DOI: 10.1088/1674-1056/21/6/064215

Nonlinear spectroscopy of three-photon excitation of cesium Rydberg atoms in vapor cell*

Jiabei Fan(樊佳蓓)[1], Yunhui He(何云辉)[1], Yuechun Jiao(焦月春)[1,2], Liping Hao(郝丽萍)[1], Jianming Zhao(赵建明)[1,2,†], and Suotang Jia(贾锁堂)[1,2]

[1] State Key Laboratory of Quantum Optics and Quantum Optics Devices, Institute of Laser Spectroscopy, Shanxi University, Taiyuan 030006, China
[2] Collaborative Innovation Center of Extreme Optics, Shanxi University, Taiyuan 030006, China

(Received 30 July 2020; revised manuscript received 13 October 2020; accepted manuscript online 13 November 2020)

We present nonlinear spectra of four-level ladder cesium atoms employing $6S_{1/2} \rightarrow 6P_{3/2} \rightarrow 7S_{1/2} \rightarrow 30P_{3/2}$ scheme of a room temperature vapor cell. A coupling laser drives Rydberg transition, a dressing laser couples two intermediate levels, and a probe laser optically probes the nonlinear spectra via electromagnetically induced transparency (EIT). Nonlinear spectra are detected as a function of coupling laser frequency. The observed spectra exhibit an enhanced absorption (EA) signal at coupling laser resonance to Rydberg transition and enhanced transmission (ET) signals at detunings to the transition. We define the enhanced absorption (transmission) strength, $H_{\rm EA}$ ($H_{\rm ET}$), and distance between two ET peaks, $\gamma_{\rm ET}$, to describe the spectral feature of the four-level atoms. The enhanced absorption signal $H_{\rm EA}$ is found to have a maximum value when we vary the dressing laser Rabi frequency $\Omega_{\rm d}$, corresponding Rabi frequency is defined as a separatrix point, $\Omega_{\rm d_{Se}}$. The values of $\Omega_{\rm d_{Se}}$ and further $\eta = \Omega_{\rm d_{Se}}/\Omega_{\rm c}$ are found to depend on the probe and coupling Rabi frequency but not the atomic density. Based on $\Omega_{\rm d_{Se}}$, the spectra can be separated into two regimes, weak and strong dressing ranges, $\Omega_{\rm d} \lesssim \Omega_{\rm d_{Se}}$ and $\Omega_{\rm d} \gtrsim \Omega_{\rm d_{Se}}$, respectively. The spectroscopies display different features at these two regimes. A four-level theoretical model is developed that agrees well with the experimental results in terms of the probe-beam absorption behavior of Rabi frequency-dependent dressed states.

Keywords: nonlinear spectroscopy, three-photon scheme, Rydberg state

PACS: 42.65.An, 32.80.Rm, 42.50.Gy **DOI:** 10.1088/1674-1056/abca25

1. Introduction

Nonlinear optical effects have played an important role in quantum optics and all-optical information processing,[1–4] especially in the field of atomic and molecular physics. A number of related techniques have been developed, including cavity coupling,[5–7] plasmas,[8] optical waveguide.[9,10] Recently, Rydberg atom has been exploited as a unique medium for investigating the nonlinear properties due to its extraordinary properties.[11] The strong long-range interaction ($\sim n^{11}$, with n principal quantum number) between Rydberg atoms has been used to achieve single photon source,[12–14] single-photon transistor,[15] cooperative enhancement of nonlinearities,[16–18] which provides an important step toward nonlinearities in quantum computation,[19] quantum gate,[20,21] and quantum information processing.[22,23] Their large polarizability and microwave-transition dipole moment have been employed to achieve a giant dc Kerr coefficient[24] and to measure the electric fields of electromagnetic radiation with a large dynamic range.[25–28]

Rydberg state can be excited by a single-photon scheme using an UV laser,[29,30] but mostly by a two-photon excition[25,31,32] for higher excitation probability. Of these approaches, the double- or triple-frequency laser is required which is expensive and intricate. In an alternative way, a multi-photon scheme, such as a three-photon excitation with inexpensive and straightforward diode lasers, has caught one's attention.[33,34] Recent experiments have demonstrated multi-photon transitions in atomic experiments,[35–37] and the nonlinear spectroscopy of Rydberg multi-photon excitation is becoming a hot topic in recent years.

In this work, we investigate, theoretically and experimentally, the three-photon nonlinear spectroscopy of cesium Rydberg atoms in a vapor cell employing electromagnetically induced transparency (EIT). The dependence of the Rydberg spectroscopy on the dressing laser Rabi frequency, $\Omega_{\rm d}$, is investigated. The obtained three-photon spectrum exhibits an enhanced absorption (EA) signal at resonance of coupling laser and two enhanced transmission (ET) signals at detuned frequencies. The enhanced absorption (transmission) strength, $H_{\rm EA}$ ($H_{\rm ET}$), and distance between two ET peaks, $\gamma_{\rm ET}$, are defined to describe the spectral characteristics. The $H_{\rm EA}$ is found to have a maximum value, corresponding dressing laser Rabi frequency is defined as separatrix, $\Omega_{\rm d_{Se}}$. Based on $\Omega_{\rm d_{Se}}$, the spectra are divided into two regimes, weak and strong dressing

*Project supported by the National Key Research and Development Program of China (Grant No. 2017YFA0304203), the State Key Program of the National Natural Science of China (Grant Nos. 11434007 and 61835007), the National Natural Science Foundation of China (Grant Nos. 61675123, 61775124, and 11804202), and the Changjiang Scholars and Innovative Research Team in University of Ministry of Education of China (Grant No. IRT_17R70).

†Corresponding author. E-mail: zhaojm@sxu.edu.cn

© 2021 Chinese Physical Society and IOP Publishing Ltd

regime. The spectroscopies display different features at these two regimes. A four-level theoretical model is developed that agrees well with experimental results.

2. Theoretical model

We consider a four-level scheme, see Fig. 1(a), consisting of a ground state $|g\rangle$, an excited state $|e\rangle$, a dressed state $|d\rangle$, and a Rydberg state $|r\rangle$. Probe laser drives the transition $|g\rangle \rightarrow |e\rangle$, corresponding Rabi frequency of $\Omega_{\rm p}$, while dressing (coupling) laser couples the transition of $|e\rangle \rightarrow |d\rangle$ ($|d\rangle \rightarrow |r\rangle$) with Rabi frequency $\Omega_{\rm d}$ ($\Omega_{\rm c}$). The probe transmission is detected with a photodiode (PD) detector, see Fig. 1(b).

In consideration of the Doppler effect, the velocity selection can be written as follows:

$$\begin{aligned} \Delta_{\rm p}\cdot h &= \Delta_{\rm p} + k_{\rm p}\cdot v, \\ \Delta_{\rm d}\cdot h &= \Delta_{\rm d} + k_{\rm d}\cdot v, \\ \Delta_{\rm c}\cdot h &= \Delta_{\rm c} + k_{\rm c}\cdot v, \end{aligned} \tag{1}$$

where h is the Planck constant, Δ_i and k_i are the detuning and wavenumbers of the lasers, respectively, and $i = {\rm p,d,c}$. The Hamiltonian of four-level system can be expressed as

$$H = \frac{\hbar}{2}\begin{pmatrix} 0 & \Omega_{\rm p} & 0 & 0 \\ \Omega_{\rm p} & -2\Delta_{\rm p} & \Omega_{\rm d} & 0 \\ 0 & \Omega_{\rm d} & -2(\Delta_{\rm p}+\Delta_{\rm d}) & \Omega_{\rm c} \\ 0 & 0 & \Omega_{\rm c} & -2(\Delta_{\rm p}+\Delta_{\rm d}+\Delta_{\rm c}) \end{pmatrix}. \tag{2}$$

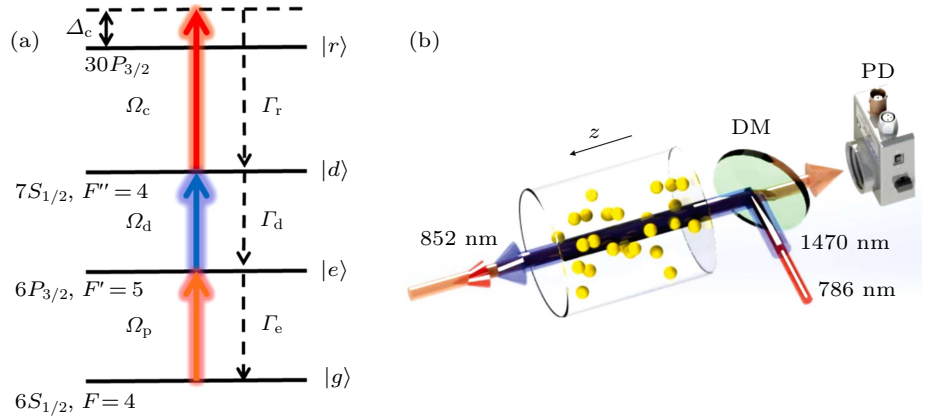


Fig. 1. (a) Diagram of a four-level system. A probe light with wavelength $\lambda_{\rm p}$ and Rabi frequency $\Omega_{\rm p}$, (a dressing light with $\lambda_{\rm d}$ and $\Omega_{\rm d}$) is locked to the resonant transition of $|6S_{1/2},F=4\rangle \rightarrow |6P_{3/2},F'=5\rangle$ ($|6P_{3/2},F'=5\rangle \rightarrow |7S_{1/2},F''=4\rangle$). A coupling laser with $\lambda_{\rm c}$ and $\Omega_{\rm c}$ is scanned through the transition of $|7S_{1/2},F''=4\rangle \rightarrow |30P_{3/2}\rangle$. $\Gamma_{\rm e}$, $\Gamma_{\rm d}$, and $\Gamma_{\rm r}$ are the decay of excited state, dressed state, and Rydberg state, respectively. (b) Sketch of the experimental setup. The coupling and dressing lasers co-propagate along z axis reflected with a DM, whereas the probe laser is set to counter-propagate to the coupling and dressing beams in the center of the cesium vapor cell. The spectroscopy of a four-level cesium atom is attained with a probe transmission detected with a PD detector as a function of the coupling laser detuning. PD: photodiode; DM: dichroic mirror.

The probe and dressing lasers are locked to the resonant transition $|g\rangle \rightarrow |e\rangle$ and $|e\rangle \rightarrow |d\rangle$ in the experiment, then we set $\Delta_{\rm p} = \Delta_{\rm d} = 0$ in calculations. Considering the decay terms, we use the Lindblad equation to describe the evolution of the density matrix ρ as follows:

$$\dot{\rho} = -\frac{\rm i}{\hbar}[H,\rho] + \mathfrak{L}, \tag{3}$$

where $\mathfrak{L}$ is the Lindblad operator considering decay term,

$$\mathfrak{L} = \begin{pmatrix} \Gamma_{\rm e}\rho_{22} & -\frac{1}{2}\Gamma_{\rm e}\rho_{12} & -\frac{1}{2}\Gamma_{\rm d}\rho_{13} & -\frac{1}{2}\Gamma_{\rm r}\rho_{14} \\ -\frac{1}{2}\Gamma_{\rm e}\rho_{21} & -\Gamma_{\rm e}\rho_{22}+\Gamma_{\rm d}\rho_{33} & -\frac{1}{2}(\Gamma_{\rm e}+\Gamma_{\rm d})\rho_{23} & -\frac{1}{2}(\Gamma_{\rm e}+\Gamma_{\rm r})\rho_{24} \\ -\frac{1}{2}\Gamma_{\rm d}\rho_{31} & -\frac{1}{2}(\Gamma_{\rm e}+\Gamma_{\rm d})\rho_{32} & -\Gamma_{\rm d}\rho_{33}+\Gamma_{\rm r}\rho_{44} & -\frac{1}{2}(\Gamma_{\rm d}+\Gamma_{\rm r})\rho_{34} \\ -\frac{1}{2}\Gamma_{\rm r}\rho_{41} & -\frac{1}{2}(\Gamma_{\rm e}+\Gamma_{\rm r})\rho_{42} & -\frac{1}{2}(\Gamma_{\rm d}+\Gamma_{\rm r})\rho_{43} & -\Gamma_{\rm r}\rho_{44} \end{pmatrix}. \tag{4}$$

For convenience, we use the state basis $\{|1\rangle,|2\rangle,|3\rangle,|4\rangle\}$ to represent $\{|g\rangle,|e\rangle,|d\rangle,|r\rangle\}$. ρ_{kj} is the density matrix element with $k,j = 1,2,3,4$. Γ_i ($i = {\rm e,d,r}$) denotes the spontaneous decay rate of $|i\rangle$ state. Here we do not include collision terms or dephasing terms due to the present study done in a vapor cell. The dephasing due to Rydberg-atom collisions can be decreased, for instance by reducing the laser intensities, decreasing laser beam waist and further the atom-field interaction time and using lower principal quantum number n, such as $n = 30$ used here. In this work, we assume the decay $|e\rangle$ to $|g\rangle$ with the rate of $\Gamma_{\rm e} = 2\pi \times 5.2$ MHz, and decay rate of the state of $|d\rangle$ and $|r\rangle$ are $\Gamma_{\rm d} = 2\pi \times 3.3$ MHz, and $\Gamma_{\rm r} = 2\pi \times 0.01$ MHz, respectively.

The spectrum is given by the probe-power transmission,

$P = P_0 \exp(-\alpha L)$, with the probe-laser absorption coefficient, $\alpha = 2\pi \mathrm{Im}(\chi)/\lambda_\mathrm{p}$, the cell length, L, and the susceptibility of the medium seen by the probe laser, χ. The susceptibility, χ, is

$$\chi = \frac{2N\mu_{12}}{E_\mathrm{p}\varepsilon_0}\rho_{12}, \tag{5}$$

where N is the average atomic density, μ_{12} is the dipole moment of transition $|1\rangle \to |2\rangle$, E_p is the amplitude of the probe, ε_0 is the vacuum permittivity, and ρ_{12} is the density matrix element between $|1\rangle$ and $|2\rangle$.

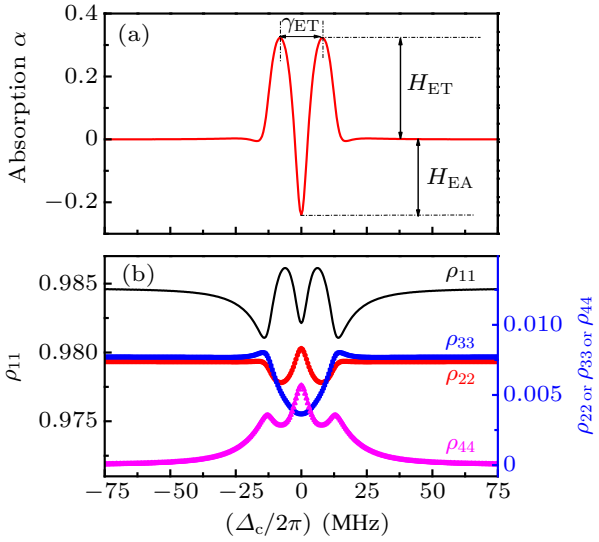


Fig. 2. Calculations of cesium four-level atom with $\Omega_\mathrm{p} = 2\pi \times 3.7$ MHz, $\Omega_\mathrm{d} = 2\pi \times 10.0$ MHz, and $\Omega_\mathrm{c} = 2\pi \times 7.7$ MHz. Decay rate is taken as $\Gamma_\mathrm{e} = 2\pi \times 5.2$ MHz, $\Gamma_\mathrm{d} = 2\pi \times 3.3$ MHz, and $\Gamma_\mathrm{r} = 2\pi \times 0.01$ MHz, respectively. (a) Calculation of the probe absorption coefficient, α. The spectrum demonstrates an enhanced absorption at the coupling resonance, $\Delta_\mathrm{c} = 0$, and two enhanced transmission peaks on both detuning sides. H_EA (H_ET) displays the signal strength of enhanced absorption (transmission) and γ_ET represents the distance between two ET peaks. (b) Populations of four levels ρ_{11} (black), ρ_{22} (red), ρ_{33} (blue), and ρ_{44} (purple) for $|g\rangle$, $|e\rangle$, $|d\rangle$, and $|r\rangle$ states as a function of the coupling laser detuning Δ_c.

Using standard semi-classical methods,[38] we numerically solve the Lindblad equation Eq. (3) in steady-state for the density matrix ρ, and further obtain populations of relative levels and the nonlinear absorption spectrum of the four-level atom. Figure 2(a) presents the calculation of absorption coefficient, α, of the four-level atom with probe laser Rabi frequency $\Omega_\mathrm{p} = 2\pi \times 3.7$ MHz and coupling (dressing) laser $\Omega_\mathrm{c} = 2\pi \times 7.7$ MHz ($\Omega_\mathrm{d} = 2\pi \times 10.0$ MHz). It is seen that the spectrum demonstrates an enhanced absorption (EA) signal on the coupling resonance and two enhanced transmission (ET) peaks on both detuned sides. This spectral profile can be explained with the dressed state picture,[34] where the four-level atom includes two ladder EIT schemes, leading to two enhanced transmission (ET) or electromagnetically induced transmission (EIT) peaks. In the resonance, two dark states overlapping in frequency domain result in an enhanced absorption due to the constructive interference. To better understand the spectral feature, we define a signal strength of absorption (transmission) relative to the background, H_EA (H_ET), to describe the enhanced absorption (transmission) of probe laser, and the distance between two ET peaks, γ_ET, as marked in the Fig. 2(a). To investigate the atomic distribution, we also plot the populations of relative levels in Fig. 2(b). It is found that most of the atoms, $\gtrsim 98.5\%$, interacting with laser beams are populated in the ground state, whereas a few atoms can be populated in the excited states near the three photon resonance. At the resonance point, only $\backsim 0.5\%$ atoms can be excited to Rydberg state.

3. Experiments and discussion

The three-photon spectral experiment is performed with a room temperature cesium vapor cell, related experimental setup is shown in Fig. 1(b). A coupling laser, λ_c and Ω_c, and a dressing laser, λ_d and Ω_d, co-propagate along z axis, which are combined with a dichroic mirror (DM). A probe laser, λ_p and Ω_p, is set to counter-propagate with dressing and coupling lasers, see Fig. 1(b). Three beams overlap with each other in the center of the vapor cell. The power of the probe beam passing through the cell is detected with a photodiode (PD) detector. The spectral signal is observed by measuring the transmission of the probe beam as a function of the coupling laser frequency.

As shown in Fig. 1(a), a weak probe laser with a wavelength $\lambda_\mathrm{p} = 852$ nm and waist $w_{\mathrm{p}0} = 350$ μm resonantly interacts with the transition $|6S_{1/2}, F = 4\rangle \to |6P_{3/2}, F' = 5\rangle$. A 1470-nm dressing laser with waist $w_{\mathrm{d}0} = 400$ μm is locked to $|6P_{3/2}, F' = 5\rangle \to |7S_{1/2}, F'' = 4\rangle$ transition with the double resonant spectroscopy of the other room temperature cell, not shown in here. While a strong coupling laser, $\lambda_\mathrm{c} = 786$ nm and $w_{\mathrm{c}0} = 200$ μm, is frequency scanned cover the $|7S_{1/2}\rangle \to |30P_{3/2}\rangle$ Rydberg transition. As mentioned above, we choose lower principal quantum number $n = 30$ for higher excitation probability of coupling transition and weak interaction between atoms, that has a negligible effect. The coupling laser power of 200 mW and corresponding Rabi frequency $\Omega_\mathrm{c} = 2\pi \times 7.7$ MHz is kept fixed. The Rabi frequency Ω_i ($i = \mathrm{p}, \mathrm{d}, \mathrm{c}$) can be calculated with the formula $\Omega_i = \mu_i E_i/\hbar$, with μ_i the transition dipole moment and E_i the amplitude of the laser beam calculated using the laser power and the beam waist. The three beams are linearly polarized, with polarizations parallel to each other.

Figure 3 presents measured spectra as a function of the coupling laser detuning, Δ_c, for the coupling (probe) Rabi frequency $\Omega_\mathrm{c} = 2\pi \times 7.7$ MHz ($\Omega_\mathrm{p} = 2\pi \times 3.7$ MHz) and three indicated Ω_d. The spectra of Fig. 3 clearly demonstrate the enhanced absorption on the coupling resonance point and two enhanced transmission peaks on both detuned sides. The spectral profiles agree with the theoretical simulations, see red solid

curves of Fig. 3. The deviation of the ET peaks of Fig. 3 middle panel is attributed to a small shift of the dressing laser frequency in the experiment, that yields an asymmetric spectral profile at both sides of coupling detuning. It is seen, from Fig. 3, that the ET peak strength, $H_{\rm ET}$, and distance of two ET peaks, $\gamma_{\rm ET}$, show increasing with the dressing laser Rabi frequency $\Omega_{\rm d}$, whereas the absorption strength, $H_{\rm EA}$, demonstrates increasing with $\Omega_{\rm d}$, (middle panel of Fig. 3), and then decrease after some value of $\Omega_{\rm d}$, (bottom panel of Fig. 3).

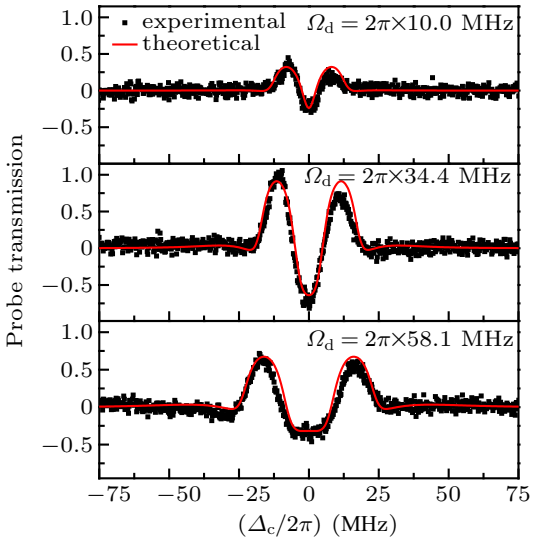


Fig. 3. Measurements (symbols) and calculations (lines) of nonlinear spectra as a function of the coupling laser frequency at coupling Rabi frequency $\Omega_{\rm c}=2\pi\times7.7$ MHz and probe Rabi frequency $\Omega_{\rm p}=2\pi\times3.7$ MHz. The spectra demonstrate an enhanced absorption on the coupling resonance and two enhanced transmission peaks on both detuned sides of the resonance.

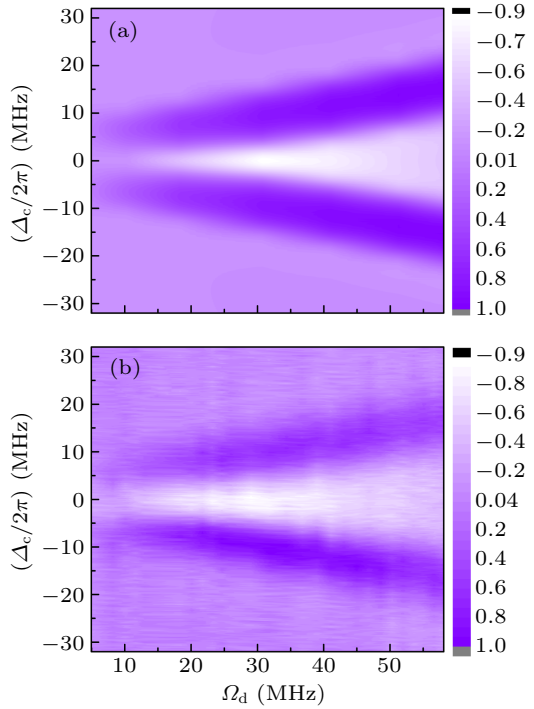


Fig. 4. Spectroscopies of four-level cesium atoms of theoretical simulations (a) and experimental measurements (b) as a function of dressing laser Rabi frequency, $\Omega_{\rm d}$, and coupling laser detuning, $\Delta_{\rm c}$. In calculations, $\Omega_{\rm p}=2\pi\times3.7$ MHz and $\Omega_{\rm c}=2\pi\times7.7$ MHz, $\Delta_{\rm d}=\Delta_{\rm p}=0$.

To understand the spectral feature above, we have carried out a series of theoretical calculations and experimental measurements such as in Fig. 3. In Fig. 4(a), we show calculations of absorption coefficient as a function of $\Omega_{\rm d}$ and $\Delta_{\rm c}$, where $\Omega_{\rm p}$ and $\Omega_{\rm c}$ are taken from experiments. For comparison, we present the measured spectroscopies in Fig. 4(b), for the case of a fixed $\Omega_{\rm p}=2\pi\times3.7$ MHz and $\Omega_{\rm c}=2\pi\times7.7$ MHz, $\Delta_{\rm d}=\Delta_{\rm p}=0$. We found that both calculations and measurements of spectra display similar spectral feature, showing a good agreement. Close inspect of the Fig. 4 reveals that the linewidth of ET peaks is invariant when $\Omega_{\rm d}$ varies, and space between two ET peaks, $\gamma_{\rm ET}$, displays slight nonlinear dependence on $\Omega_{\rm d}$.

From Fig. 4, we extract the ET (EA) signal strength $H_{\rm ET}$ ($H_{\rm EA}$) and space of two ET peaks, $\gamma_{\rm ET}$, to characterize the spectroscopy of four-level atoms. Figure 5 presents measurements (symbols) and calculations (lines) of $\gamma_{\rm ET}$ and $H_{\rm ET}$ ($H_{\rm EA}$) as a function of the dressing laser $\Omega_{\rm d}$ for different coupling laser $\Omega_{\rm c}$. It is found that the data of measurements are mostly sitting in the red lines, the case of $\Omega_{\rm c}=2\pi\times7.7$ MHz of calculations, demonstrating that the measurements are consistent with the calculations.

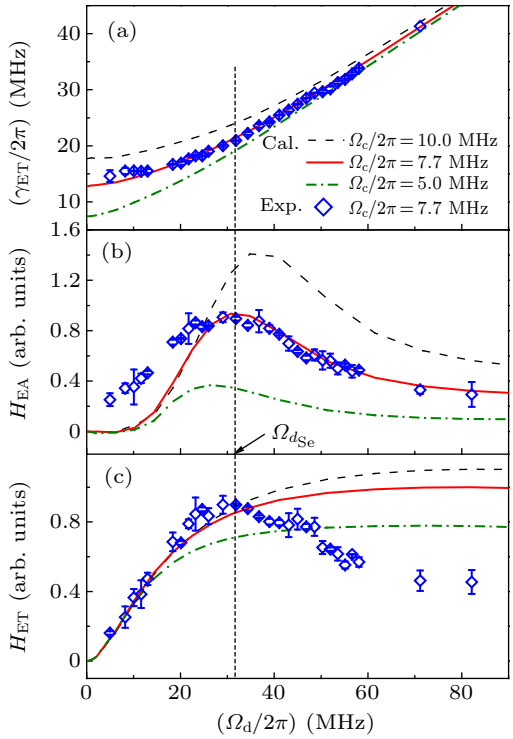


Fig. 5. Measurements (symbols) and calculations (lines) of $\gamma_{\rm ET}$ (a), $H_{\rm EA}$ (b), and $H_{\rm ET}$ (c), as a function of $\Omega_{\rm d}$. The parameters of calculations are the same as those in Fig. 4 but different $\Omega_{\rm c}=2\pi\times7.7$ MHz (red solid line), $2\pi\times10.0$ MHz (black dashed line), and $2\pi\times5.0$ MHz (green dot-dashed line), respectively. As estimated, the data of measurements for coupling laser $\Omega_{\rm c}=2\pi\times7.7$ MHz are mostly sitting in the red line. A vertical dashed line marks the separatrix dressing laser Rabi frequency $\Omega_{\rm d_{Se}}$ for the case of $\Omega_{\rm c}=2\pi\times7.7$ MHz, at which value the enhanced absorption $H_{\rm EA}$ has a maximum value $H_{\rm EA_{max}}$. $\Omega_{\rm d_{Se}}$ displays increase with $\Omega_{\rm c}$. For fixed $\Omega_{\rm c}$, the vertical dashed line separates the spectra into two regimes, strong (weak) dressing regime, corresponding to $\Omega_{\rm c}\gtrsim\Omega_{\rm d_{Se}}$ ($\Omega_{\rm c}\lesssim\Omega_{\rm d_{Se}}$), see text for details. In calculations, $\Omega_{\rm p}=2\pi\times3.7$ MHz and $\Delta_{\rm c}=\Delta_{\rm p}=0$.

We firstly discuss H_{EA} feature of Fig. 5(b). It is seen that there is a maximum value $H_{EA_{max}}$ when we vary Ω_d, corresponding dressing Rabi frequency is defined as a separatrix dressing Rabi frequency, $\Omega_{d_{Se}}$. For instance $\Omega_{d_{Se}} = 2\pi\times30.7$ MHz for the case of $\Omega_c = 2\pi \times 7.7$ MHz and $\Omega_p = 2\pi \times 3.7$ MHz, as denoted with an arrow and a vertical dashed line. The vertical dashed line separates the spectra into two regimes, strong and weak dressing regimes, corresponding $\Omega_d \gtrsim \Omega_{d_{Se}}$ and $\Omega_d \lesssim \Omega_{d_{Se}}$, respectively. The H_{EA} displays increasing with Ω_d at the weak dressing regime and decreasing with Ω_d at the strong dressing regime. It is also seen that the $\Omega_{d_{Se}}$ strongly depends on the coupling laser Ω_c, showing increase with Ω_c, therefore we define the ratio $\eta = \Omega_{d_{Se}}/\Omega_c$. To understand the maximum H_{EA}, we also calculate absorption coefficient per velocity classes for different Ω_c and Ω_d and for fixed the probe Ω_p, not shown here. The calculations reveal that the resonance absorption becomes velocity insensitive at the appropriate ratio of Ω_d/Ω_c, that leads to more atoms contribute to the signal and therefore the maximum absorption H_{EA} at resonant of dressing laser.[36] From Fig. 5(b), $\eta = 3.72$, 3.98, and 4.80 for $\Omega_c/2\pi = 10$ MHz, 7.7 MHz, and 5 MHz, respectively. The value of η varies as the coupling Ω_c is changed. To investigate the dependence of the $\Omega_{d_{Se}}$ on the probe Ω_p and the atomic density, in Fig. 6, we present calculations of the enhanced absorption H_{EA} as a function of Ω_d with $\Omega_c = 2\pi\times$ 7.7 MHz and indicated probe Ω_p of Fig. 6(a) and atomic density of Fig. 6(b). It is clear that $\Omega_{d_{Se}}$ also depends on the probe laser Ω_p (Fig. 6(a)) but not the atomic density (Fig. 6(b)).

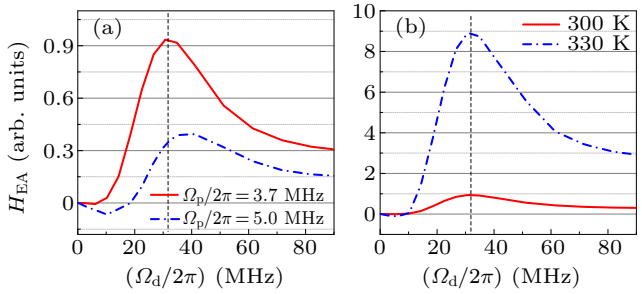


Fig. 6. (a) Calculations of the enhanced absorption H_{EA} as a function of Ω_d with $\Omega_c = 2\pi \times 7.7$ MHz at room temperature (300 K) and an indicated probe laser $\Omega_p/2\pi = 3.7$ MHz (red solid line) and 5.0 MHz (blue dashed-dot line). The extracted $\Omega_{d_{Se}}$ and the ratio η increase with the probe Rabi frequency. (b) The same calculations like in panel (a) with $\Omega_c = 2\pi \times 7.7$ MHz and $\Omega_p = 2\pi \times 3.7$ MHz for the cell temperature 300 K (red solid line) and 330 K (blue dashed-dot line), related atomic density of 1.4×10^{10} cm^{-3} and 2.3×10^{11} cm^{-3}, respectively. The enhanced absorption H_{EA} strongly depends on the atomic density but $\Omega_{d_{Se}}$ and the ratio η show independence of the atomic density. Vertical dashed lines mark the position of $\Omega_{d_{Se}}$ of the case of $\Omega_p = 2\pi \times 3.7$ MHz.

We then discuss the spectral features of two regimes. In the weak dressing regime, H_{ET} and H_{EA} display increase with Ω_d while less independent of Ω_c. However, the distance between two ET peaks, γ_{ET}, shows slightly increase with Ω_d but strongly depends on Ω_c. While in the strong dressing regime, H_{EA} (H_{ET}) is dependent on the coupling Ω_c and decrease (saturations) when Ω_d increases further. However, γ_{ET} shows linear dependence on Ω_d and almost independent of the Ω_c and gradually converge in greater Ω_d. For negative value of H_{EA} of $\Omega_d/2\pi < 20$ MHz range, see blue dashed line of Fig. 6(a), the calculated spectrum under these probe and coupling laser condition has only two ET peaks without absorption at resonance, related the transition of the probe beam at resonance larger than background. It should be noted from Fig. 5(c), that enhanced transmission, H_{ET}, shows an increase with Ω_d and tends to saturate in calculations, but declines in measurement. The difference between measurement and calculation for $\Omega_d \gtrsim \Omega_{d_{Se}}$ is attributed to the splitting and line broadening of two ET peaks in higher dressed field in experiments, see Fig. 4(b), due to inhomogeneity of interaction between atom and laser field.[39]

4. Conclusion

We have demonstrated the nonlinear spectra of a four-level ladder cesium atom with up level involving Rydberg state. Results are modeled by numerically solving the Lindblad equation in terms of the probe-beam absorption behavior of Rabi frequency-dependent dressed states. For the sake of convenience, we define γ_{ET} as the distance between two ET peaks and H_{EA} (H_{ET}) as the signal strength of enhanced absorption (transmission). The calculations reproduce well the experimental spectra of the four-level atom. We have defined a separatrix dressing laser $\Omega_{d_{Se}}$, based on which the spectra are separated into two regions. An enhanced absorption (transmission) strength, H_{EA} (H_{ET}), shows increasing with Ω_d in the weak dressing range of $\Omega_d \lesssim \Omega_{d_{Se}}$, and decreasing (saturation) in the strong dressing range of $\Omega_d \gtrsim \Omega_{d_{Se}}$. For the distance between two ET peaks, γ_{ET}, strongly depends on the coupling Ω_c in the weak dressing range and linear increasing with dressing laser Ω_d in strong dressing range. More calculations indicate that $\Omega_{d_{Se}}$ and further η depends on the probe and coupling laser Rabi frequency but independence of the atomic density. The three-photon Rydberg-EIT with low cost all-infrared laser diode systems can access to the Rydberg state, which could be valuable for Rydberg-atom based microwave[35] and THz measurement.[40]

References

[1] Bloembergen N 1982 *Rev. Mod. Phys.* **54** 685
[2] Shen Y R 1976 *Rev. Mod. Phys.* **48** 1
[3] Zhang Z D, Wang K, Yi Z H, Zubairy M S, Scully M O and Mukamel S 2019 *J. Phys. Chem. Lett.* **10** 4448
[4] Dorfman K E and Mukamel S 2018 *Proc. Natl. Acad. Sci. USA* **115** 1451
[5] Begley S, Vogt M, Gulati G K, Takahashi H and Keller M 2016 *Phys. Rev. Lett.* **116** 223001
[6] Casabone B, Friebe K, Brandstätter B, Schüppert K, Blatt R and Northup T E 2015 *Phys. Rev. Lett.* **114** 023602

[7] Hoffman A J, Srinivasan S J, Gambetta J M and Houck A A 2011 *Phys. Rev. B* **84** 184515
[8] Bernstein I B, Greene J M and Kruskal M D 1957 *Phys. Rev.* **108** 546
[9] Olshansky R 1979 *Rev. Mod. Phys.* **51** 341
[10] Alexeeva N V, Barashenkov I V, Rayanov K and S Flach 2014 *Phys. Rev. A* **89** 013848
[11] Gallagher T F 1994 *Rydberg Atoms* (New York: Cambridge University Press)
[12] Brattke S, Varcoe B T H and Walther H 2001 *Phys. Rev. Lett.* **86** 3534
[13] Dudin Y O and Kuzmich A 2012 *Science* **336** 887
[14] Viscor D, Li W B and Lesanovsky I 2015 *New J. Phys.* **17** 033007
[15] Gorniaczyk H, Tresp C, Schmidt J, Fedder H and Hofferberth S 2014 *Phys. Rev. Lett.* **113** 053601
[16] Busche H, Huillery P, Ball S W, Ilieva T, Jones M P A and Adams C S 2017 *Nat. Phys.* **13** 655
[17] Pritchard J D, Maxwell D, Gauguet A, Weatherill K J, Jones M P A and Adams C S 2010 *Phys. Rev. Lett.* **105** 193603
[18] Petrosyan D, Otterbach J and Fleischhauer M 2011 *Phys. Rev. Lett.* **107** 213601
[19] Saffman M, Walker T G and Mølmer K 2010 *Rev. Mod. Phys.* **82** 2313
[20] Jaksch D, Cirac J I, Zoller P, Rolston S L, Côté R and Lukin M D 2000 *Phys. Rev. Lett.* **85** 2208
[21] Isenhower L, Urban E, Zhang X L, Gill A T, Henage T, Johnson T A, Walker T G and Saffman M 2010 *Phys. Rev. Lett.* **104** 010503
[22] Lukin M D, Fleischhauer M, Côté R, Duan L M, Jaksch D, Cirac J I and Zoller P 2001 *Phys. Rev. Lett.* **87** 037901
[23] Galindo A and Martín-Delgado M A 2002 *Rev. Mod. Phys.* **74** 347
[24] Mohapatra A K, Bason M G, Butscher B, Weatherill K J and Adams C S 2008 *Nat. Phys.* **4** 890
[25] Jiao Y C, Hao L P, Han X X, Bai S Y, Raithel G, Zhao J M and Jia S T 2017 *Phys. Rev. Appl.* **8** 014028
[26] Abel R P, Carr C, Krohn U and Adams C S 2011 *Phys. Rev. A* **84** 023408
[27] Sedlacek J A, Schwettmann A, Kübler H, Löw R, Pfau T and Shaffer J P 2012 *Nat. Phys.* **8** 819
[28] Holloway C, Gordon J A, Jefferts S, Schwarzkopf A, Anderson D A, Miller S A, Thaicharoen N and Raithel G 2014 *IEEE Trans. Antennas Propag.* **62** 6169
[29] Hankin A M, Jau Y Y, Parazzoli L P, Chou C W, Armstrong D J, Landahl A J and Biedermann G W 2014 *Phys. Rev. A* **89** 033416
[30] Wang J Y, Bai J D, He J and Wang J M 2017 *Opt. Express* **25** 22510
[31] Hao L P, Jiao Y C, Xue Y M, Han X X, Bai S Y, Zhao J M and Raithel G 2018 *New J. Phys.* **20** 073024
[32] Mohapatra A K, Jackson T R and Adams C S 2007 *Phys. Rev. Lett.* **98** 113003
[33] Carr C, Tanasittikosol M, Sargsyan A, Sarkisyan D, Adams C S and Weatherill K J 2012 *Opt. Lett.* **37** 3858
[34] Kondo J M, Šibalić N, Guttridge A, Wade C G, De Melo N R, Adams C S and Weatherill K J 2015 *Opt. Lett.* **40** 5570
[35] Thaicharoen N, Moore K R, Anderson D A, Powel R C, Peterson E and Raithel G 2019 *Phys. Rev. A* **100** 063427
[36] Wade C G, Šibalić N, de Melo N R, Kondo J M, Adams C S and Weatherill K J 2017 *Nat. Photon.* **11** 40
[37] Vogt T, Viteau M, Zhao J M, Chotia A, Comparat D and Pillet P 2006 *Phys. Rev. Lett.* **97** 083003
[38] Cohen-Tannoudji C, Dupont-Roc J, Grynberg G and Meystre P 1992 *Phys. Today* **45** 115
[39] Fan J B, Jiao Y C, Hao L P, Xue Y M, Zhao J M and Jia S T 2018 *Acta Phys. Sin.* **67** 093201 (in Chinese)
[40] Downes L A, MacKellar A R, Whiting D J, Bourgenot C, Adams C S and Weatherill K J 2020 *Phys. Rev. X* **10** 011027